Insights into Proton Recombination in Ceramic Proton Conducting Electrodes

Journal of The Electrochemical Society, 2021 **168** 044522
1945-7111/2021/168(4)/044522/5/$40.00 © 2021 The Electrochemical Society ("ECS"). Published on behalf of ECS by IOP Publishing Limited

Insights into Proton Recombination in Ceramic Proton Conducting Electrodes

Jian Chang,[1,*] Colin Lehman,[1,*] John M. Vohs,[1] Raymond J. Gorte,[1,,z] Aleksandra Vojvodic,[1] Kunli Yang,[2] and Steven McIntosh[2]**

[1]*Chemical and Biomolecular Engineering,University of Pennsylvania, Philadelphia, Pennsylvania 19104, United States of America*
[2]*Chemical and Biomolecular Engineering, Lehigh University, Bethlehem, Pennsylvania 18015, United States of America*

The effect of catalyst addition on H_2 evolution from composite electrodes of $La_{0.7}Sr_{0.3}TiO_3$ (LST) and $BaZr_{0.1}Ce_{0.7}Y_{0.1}Yb_{0.1}O_{3-\delta}$ (BZCYYb) was studied. Starting with symmetric cells (LST||BZCYYb||LST), Pt was added to one or both electrodes, after which i–V polarization measurements were performed in humidified H_2 at 723 and 773 K. The base cells showed very high impedances but these decreased dramatically upon addition of Pt to both electrodes. When Pt was added to only one electrode, the cells performed as diodes, showing that Pt was necessary for H_2 dissociation but not for H recombination. The effects of adding Ru, W, Re and Fe were also studied. DFT calculations helped confirm that H recombination on $BaZrO_3$ is expected to be barrierless. The implications of these results for potential application to electrochemical synthesis of ammonia are discussed.
 [DOI: 10.1149/1945-7111/abf79e]

Manuscript submitted February 22, 2021; revised manuscript received March 27, 2021. Published April 22, 2021.

Electrochemical production of commodity chemicals, like ammonia, is potentially very attractive. Whereas conventional production usually requires large-scale plants to be efficient, electrochemical synthesis could be scaled to smaller sizes while maintaining high energy efficiency. Proton-conducting ceramics (PCC), like $BaZr_{0.1}Ce_{0.7}Y_{0.1}Yb_{0.1}O_{3-\delta}$ (BZCYYb), are of particular interest because they exhibit reasonable conductivities in a temperature range that is similar to that used in heterogeneously catalyzed synthesis of ammonia. It is therefore not surprising that significant effort has gone into developing electrodes to do this chemistry.[1–3] However, while evidence for ammonia production has been reported, the production rates and Faradaic efficiencies that have been achieved to date are not sufficient for practical applications.

A major problem is that the transition metals commonly used in PCC, such as Ni and Pt, are excellent hydrogen-recombination catalysts and poor N_2-dissociation catalysts. This implies that the primary product from pumping hydrogen through the electrolyte into a N_2 atmosphere will be H_2. Incorporating an NH_3-synthesis catalyst such as Fe or Ru[4] into the electrode can increase NH_3 production by catalyzing conventional Haber-Bosch chemistry; however, equilibrium product yields will still be very low. Conventional Haber-Bosch synthesis is performed at very high pressures, typically greater than 250 bar, in order to push equilibrium towards the product. Even at these pressures, single-pass conversions are usually less than 20%.[5]

To circumvent these problems, we propose using an electrode that achieves electronic conductivity from a conducting oxide that is a poor hydrogen-recombination catalyst. By adding a metal that dissociates N_2 readily, such as Mo or W,[6,7] it might then be possible to electrochemically drive protons onto the metal and react away adsorbed nitrogen in the form of ammonia. The use of an electrochemical driving force enables both tuning of the hydrogen potential at the catalyst surface and the imposition of large driving forces. For example, an increase in the overpotential of just 0.1 V at 773 K leads to a nearly 1000-fold increase in the effective H_2 pressure. Evidence supporting the idea that ions from the electrolyte can spillover to react with adsorbed species on the electrode has already been reported for oxygen-anion conducting electrochemical cells. For example, Imbihl and coworkers demonstrated that oxygen ions from the electrolyte were able to remove carbonaceous species from a Pt electrode at relatively low temperatures.[8] In another study, electrochemically pumped oxygen was used to catalyze propene to acrolein on an electrode that had Cu for electronic conductivity and molybdena as a catalyst.[9] This latter example also demonstrated that separate materials can be used to achieve electronic conductivity and catalytic activity.

Another example in which electronic conductivity and catalytic function were performed by separate materials comes from work using $La_{0.7}Sr_{0.3}TiO_3$ (LST) as the anode in a solid oxide fuel cell (SOFC).[10] In the absence of a catalyst, this cell showed a maximum power density of 0.015 W cm^{-2} at 1073 K. Upon the addition of 0.5 wt% Pd onto the LST, the power density increased to 0.77 W cm^{-2}. The low loading of Pd in this example is clearly not providing electronic conductivity and the large improvement in electrode performance must be due to the ions from the electrolyte being channeled onto the Pd particles on the electrode surface.

In the present study, we examined the performance of LST-based electrodes on PCC using a BZCYYb electrolyte. The results demonstrate that a catalyst is indeed required for H_2 dissociation; however, both theory and experiment suggest that hydrogen recombination can occur in the absence of a catalytic metal.

Experimental

The BZCYYb ($BaZr_{0.1}Ce_{0.7}Y_{0.1}Yb_{0.1}O_{3-\delta}$) powder was prepared by solid-state reaction with stoichiometric amounts of barium carbonate, zirconium oxide, cerium oxide, yttrium oxide, and ytterbium oxide (all from Alfa Aesar). The mixture was ball milled in ethanol for 24 h, dried, and then pressed into pellets. The pellets were placed in a crucible together with sacrificial barium carbonate powder and calcined at 1573 K for 2 h. The BZCYYb pellets were then crushed, mixed with dispersants and binders, and cast into two green tapes, one with and one without graphite pore formers. Details on the tape-casting procedures and recipes are reported elsewhere.[11] Circular wafers were cut out of the tape that did not have pore formers, after which smaller circular wafers of the tape with pore formers were laminated onto either side. Firing at 1673 K for 2 h resulted in BZCYYb wafers with a porous-dense-porous structure. The electrolyte thicknesses were 130 μm, with 35-μm porous layers on either side. The wafers were 1.0 cm in diameter but the areas of the porous layers were only 0.5 cm^2.

To prepare the LST electrodes, concentrated, aqueous solutions of $La(NO_3)_3{\cdot}6H_2O$, $Sr(NO_3)_2$, and $[CH_3CH(O\text{-})CO_2{\cdot}NH_4]_2{\cdot}Ti(OH)_2$ [dihydroxybis(ammonium lactate)titanium(IV)] (all from Alfa Aesar) were infiltrated into both porous layers, after which the cells were heated to 723 K to form a mixed oxide with a stoichiometry of $La_{0.7}Sr_{0.3}TiO_3$. This step was repeated 7 times, after which the cells

*Electrochemical Society Student Member.
**Electrochemical Society Fellow.
[z]E-mail: gorte@seas.upenn.edu

were calcined in air at 1373 K for 4 h to form the LST perovskite phase. Catalysts were also added to one or both electrodes by one infiltration cycle of dilute aqueous solutions of their corresponding precursors, either $Pt(NH_3)_4(NO_3)_2$ (Alfa Aesar), $Ru(NO)(NO_3)_3$ (Alfa Aesar), $Fe(NO_3)_3$ (Sigma-Aldrich), NH_4ReO_4 (Sigma-Aldrich), $(NH_4)_6W_{12}O_{39}$ (Alfa Aesar). In each case, the amount of added catalyst corresponded to significantly less than 1-wt% of the electrodes and had no effect on the conductivities. After addition of catalyst precursors, the cells were heated to 723 K to decompose the precursors.

The cell structures and morphologies were analyzed using scanning electron microscopy (SEM) and X-ray diffraction (XRD). The electrochemical characteristics were measured in a single chamber with humidified H_2. While humidification is necessary for proton conduction in the BZCYYb electrolyte, switching to dry H_2 during the experiment did not affect the impedance measurements, demonstrating that H_2O does not play a major role in the electrode reactions. Silver wire and paste were attached to both electrodes. A Gamry Instruments potentiostat was used to measure both impedance spectra and i–V polarization curves.

The computations used the Atomic Simulation Environment (ASE)[12] and all DFT calculations are performed using Quantum Espresso's implementation of generalized gradient approximation (GGA) DFT[13] using the Perdew-Burke-Ernzerh (PBE) exchange-correlation functional[14] and a plane wave cutoff of 500 eV. A 3 × 3 × 1 Monkhorst-Pack grid[15] is used for k-point sampling on all relaxations. Periodic boundary conditions are implemented with a dipole correction.[16] All calculations are converged to 10^{-5} eV and forces are converged to 0.03 eV $Å^{-1}$. Core electrons are treated using ultrasoft pseudopotentials.[17] Fermi–Dirac smearing is used with a smearing width of 0.1 eV. Calculations are not spin-polarized. Activation barriers are calculated using the Nudged Elastic Band (NEB) method.[18,19] NEB calculations are considered to be converged when the forces on all atoms across images are less than 0.1 eV/Å. Free energies are calculated by correcting the DFT calculated energies with zero point energies (ZPE) and entropic effects as shown in Eq. 1. All reported free energies in this paper are calculated at T = 800 K.

$$\Delta G = \Delta E + \Delta ZPE - T\Delta S \quad [1]$$

The $BaZrO_3$ lattice parameter was calculated to be 4.207 Å in good agreement with experimental results. The [001] surface was created by repeating the unit cell to form a 2 × 2 slab and 4 unit cells are repeated in the z-direction for a total of 8 atomic layers. The bottom four layers are fully constrained and the top four layers are allowed to relax.

Results

Figure 1 shows SEM cross sectional images of the BZCYYb wafers. The lower resolution image in Fig. 1a demonstrates that the electrolyte is dense and uniform in thickness. Higher resolution images of the BZCYYb scaffold, with and without LST and taken near the electrolyte interface, are shown in Figs. 1b and 1c respectively. They indicate that the BZCYYb scaffold has regular pores, approximately 1 to 10 μm in size. The infiltrated LST forms a porous coating over the scaffold surface, roughly 2 μm thick. XRD patterns of the electrode scaffold, with and without LST, are shown in Fig. 2. The BZCYYb is free of impurity phases. After infiltration, peaks associated with the LST phase are nearly as intense as those of the BZCYYb phase. There is no indication from XRD of any solid-state reaction between the two components.

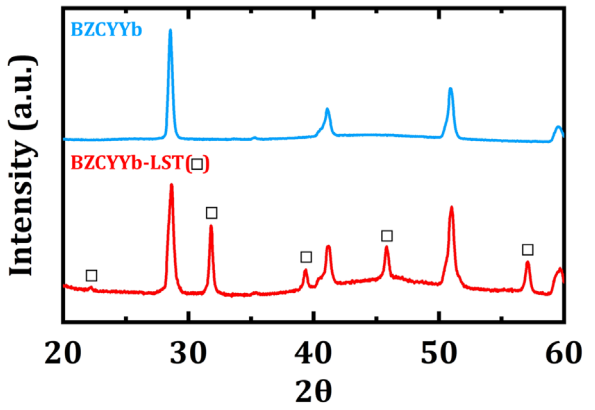

Figure 2. XRD patterns of the BZCYYb scaffolds with and without LST.

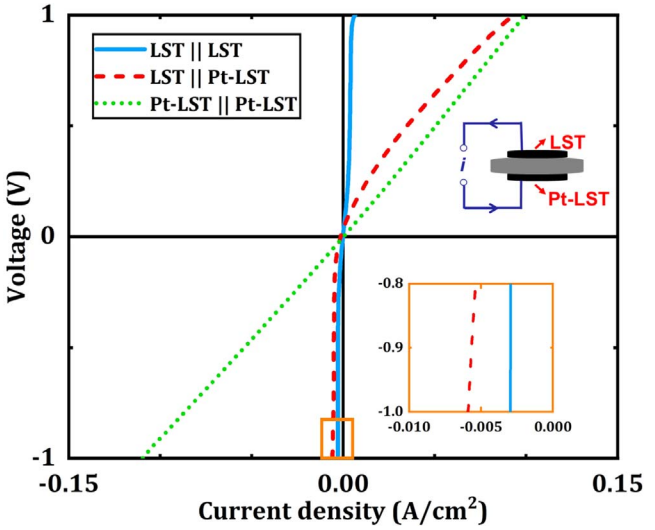

Figure 3. i–V polarization curves for the LST-BZCYYb cells with and without Pt added to the electrodes at 773 K. Scan rate was 0.01 V s^{-1}. In the case of LST||Pt-LST, the current direction is shown in the insert.

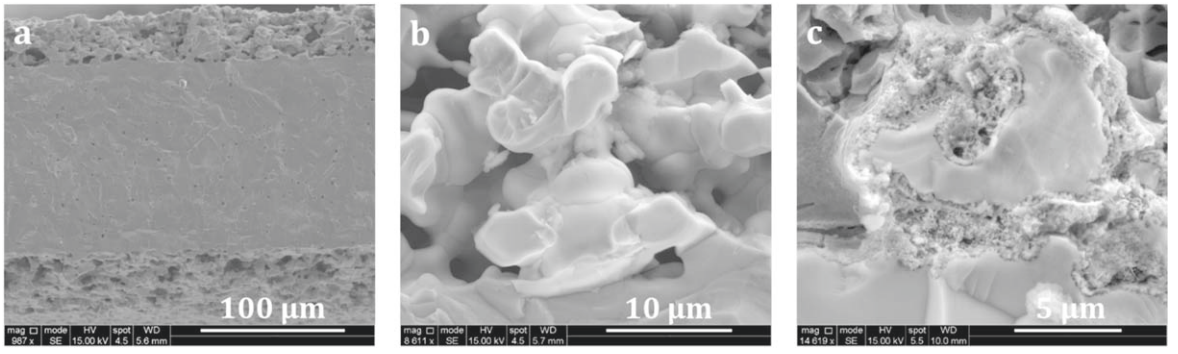

Figure 1. Microstructure of the BZCYYb wafers before and after the infiltration of LST into the electrodes. (a) cross section, (b) BZCYYb scaffold without LST and (c) BZCYYb scaffold with LST.

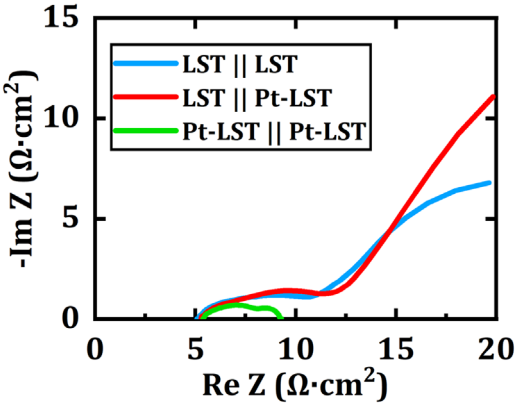

Figure 4. Electrochemical impedance spectra of the LST-BZCYYb cells with and without Pt added to the electrodes at 773 K.

To understand the performance of these electrodes and the effect of adding various catalysts, i–V polarization curves and impedance measurements were performed on cells in which both electrodes were exposed to humidified (3% H_2O) H_2. To ensure that the LST phase was conductive, the cells were initially exposed to dry H_2 for 1 h at 973 K. Figures 3 and 4 show i–V polarization curves and open-circuit impedance spectra at 773 K for three particular cells that demonstrate the range of observed behavior. First, the symmetric cell in which no catalyst was added to either LST-BZCYYb electrode shows almost no current upon polarization in either direction. At 1.0 V, the maximum current density was less than 0.003 A cm^{-2}, corresponding to an average slope of greater than 300 $\Omega{\cdot}cm^2$. As demonstrated by the impedance data in Fig. 4, the high impedance in this cell is due primarily to the poor catalytic properties of the electrodes, since the ohmic resistance was only 5 $\Omega{\cdot}cm^2$. Assuming the ohmic resistance is entirely from the 130-μm BZCYYb electrolyte, this value implies that the conductivity of BZCYYb at 773 K is 0.0026 s cm^{-1}. This is in reasonable agreement with published values for this temperature[20]; therefore, most of the ohmic contribution in these cells must come from the electrolyte, although some small contribution from the electrodes cannot be ruled out.

The addition of ~0.2-wt% Pt to each of the LST electrodes leads to a dramatic change in the performance of the cell. The i–V curve is now a straight line with maximum currents of approximately 0.11 A cm^{-2} at ±1.0 V, corresponding to a total cell impedance of approximately 9 $\Omega{\cdot}cm^2$. Impedance data in Fig. 4 indicate that adding Pt had no effect on the ohmic resistance and that the decreased cell impedance is due entirely to the non-ohmic contribution. Considering that two electrodes contribute, the impedance of each electrode was only 2 $\Omega{\cdot}cm^2$.

More interesting is what happens when Pt is added to only one of the LST-BZCYYb electrodes. The i–V curve now takes on characteristics of a diode, with current only able to flow from the electrode containing Pt to the opposite side. This suggests that Pt is required to dissociate H_2 for injection into the electrolyte as H^+ ions. However, on the opposite electrode, hydrogen recombination can occur on the LST-BZCYYb, even in the absence of Pt. The total impedance of this cell at open circuit is not well defined because of the discontinuity in the polarization curve but the ohmic resistance was again 5 $\Omega{\cdot}cm^2$.

To understand the effects of other catalytic metals, we prepared cells with Pt on one side and either W, Re, Fe, or Ru on the other. These metals were chosen because they are effective at N_2 dissociation (e.g. W, Re)[6,21] or are very good ammonia-synthesis catalysts. The i–V polarization curves for these fuel cells are shown in Fig. 5 for 723 K and 773 K. When Ru is added, the performance is nearly identical to that achieved with Pt. This is not surprising given that Ru is an excellent hydrogenation catalyst and therefore effective at H_2 dissociation. On the opposite extreme, the addition of W had no effect. Because W will exist in an oxidized form in humidified H_2, experiments were also performed in dry H_2 after reducing the electrode at 973 K, but this did not change the performance. The addition of Fe or Re gave results that were intermediate between Ru and W, suggesting that they are able to dissociate H_2 but at much lower rates than that of either Ru or Pt. They were effective only at low anodic current densities.

For purposes of the present application, it would be desirable for there to be a significant overpotential on the H_2-evolution electrode. As demonstrated in Fig. 3, the overpotential for LST-BZCYYb electrodes was already low for this direction of the current, even in the absence of a catalytic metal. In order to explain this, we performed DFT calculations to probe the underlying physics. LST was modeled as $SrTiO_3$ (STO) and BZCYYb as $BaZrO_3$ (BZO). Although the experimental electrodes are mixed oxides formed by infiltration of the LST into the porous BZCYYb layer, we modeled H binding on the BZO and STO surfaces separately. While including the electrode material interfaces in the DFT model would be informative, it would be computationally demanding, and the general binding energy trends discussed below would still be valid. We modeled the Pt infiltrated electrode by using a Pt adatom adsorbed in its most stable position on the BZO [001] facet. Although this is not likely the experimental Pt atom configuration, it allows us to easily probe Pt in contact with BZO and its effect on H binding relative to the clean surface.

Figure 6a shows the free energy diagram for a proton (1) diffusing out from the electrolyte (BZO) bulk onto the lowest energy surface binding site on either BZO, STO, or Pt and (2) recombining and evolving into the gas phase. It illustrates the different energy paths a proton can take depending on the electrode materials present. In order to generate the free energy diagram, we modeled hydrogen bound to an oxygen ion in the electrolyte (BZO) bulk cell and used this as the starting point for all of the curves. Energies for H adsorbed on the surface were determined by finding the lowest energy binding site on the AO and BO_2 terminations of the [001] facet for both STO and BZO. Only the most favorable H binding surface termination is included in the figure for clean STO and BZO. We also examined the effect of having Pt on the electrode by adsorbing H on the Pt AO and Pt BO_2 surfaces and finding the lowest energy binding site in the same way as for the clean surfaces. In order to include kinetics, we used NEB to calculate the activation barrier for hydrogen dissociation/recombination. The lowest energy structure with two H atoms adsorbed on the surface was used as the initial image for the NEB calculation. A H_2 molecule was placed above the clean surface and its lowest energy configuration was used as the final image. NEB was then used to find the transition-state configuration between these two images.

The free energy diagram in Fig. 6a allows us to make several important observations. First consider the cell shown schematically in Fig. 6b in which protons are pumped successfully from the Pt electrode to the LST electrode. The Pt AO and Pt BO_2 curves in Fig. 6a show that dissociation of H_2 is barrierless for Pt supported on both terminations of [001] BZO. The ΔG for this step is 0 eV for Pt supported on the AO termination and −0.1 eV for Pt supported on the BO_2 termination. Therefore, hydrogen dissociation on Pt supported on [001] BZO is kinetically facile and thermodynamically favored. The curve for STO shows that there is more than a 2 eV activation barrier for hydrogen evolution on [001] STO confirming that the LST electrode is not catalytic. Finally, the curve for BZO shows that hydrogen in the gas phase is 2.6 eV *more* stable than hydrogen bound to oxygen ions in the BZO bulk and 1.2 eV more stable than hydrogen adsorbed on the BZO surface. This confirms that protons in the bulk spontaneously migrate to the electrolyte surface and recombine to form H_2 gas.

We next consider the cell shown schematically in Fig. 6c in which protons cannot be pumped from the LST electrode to the Pt electrode. We are able to explain this by again looking at Fig. 6a.

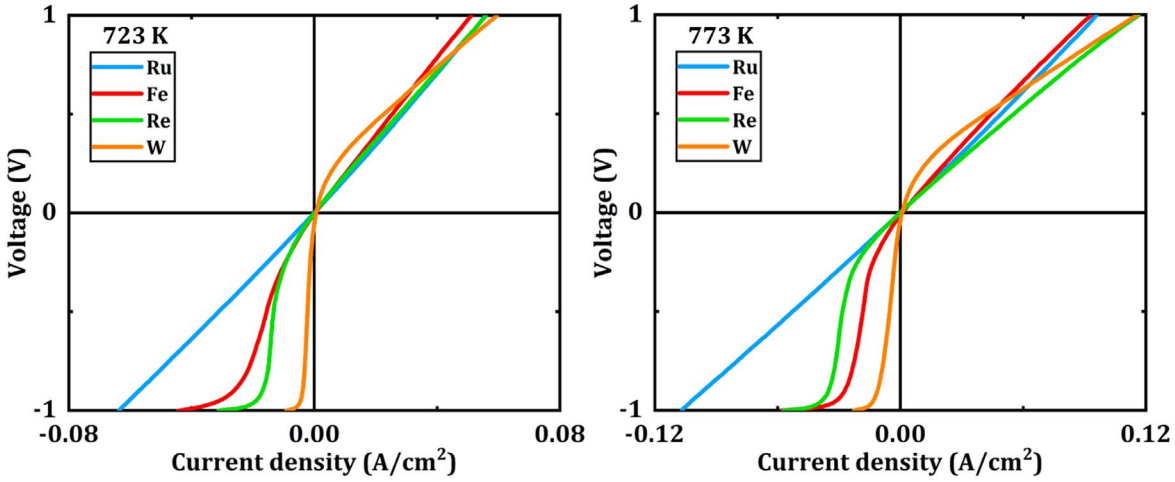

Figure 5. i–V polarization curves for the LST-BZCYYb cells with Pt on one side and either W, Re, Fe or Ru on the other at 723 K and 773 K. Scan rate was 0.01 V s^{-1}.

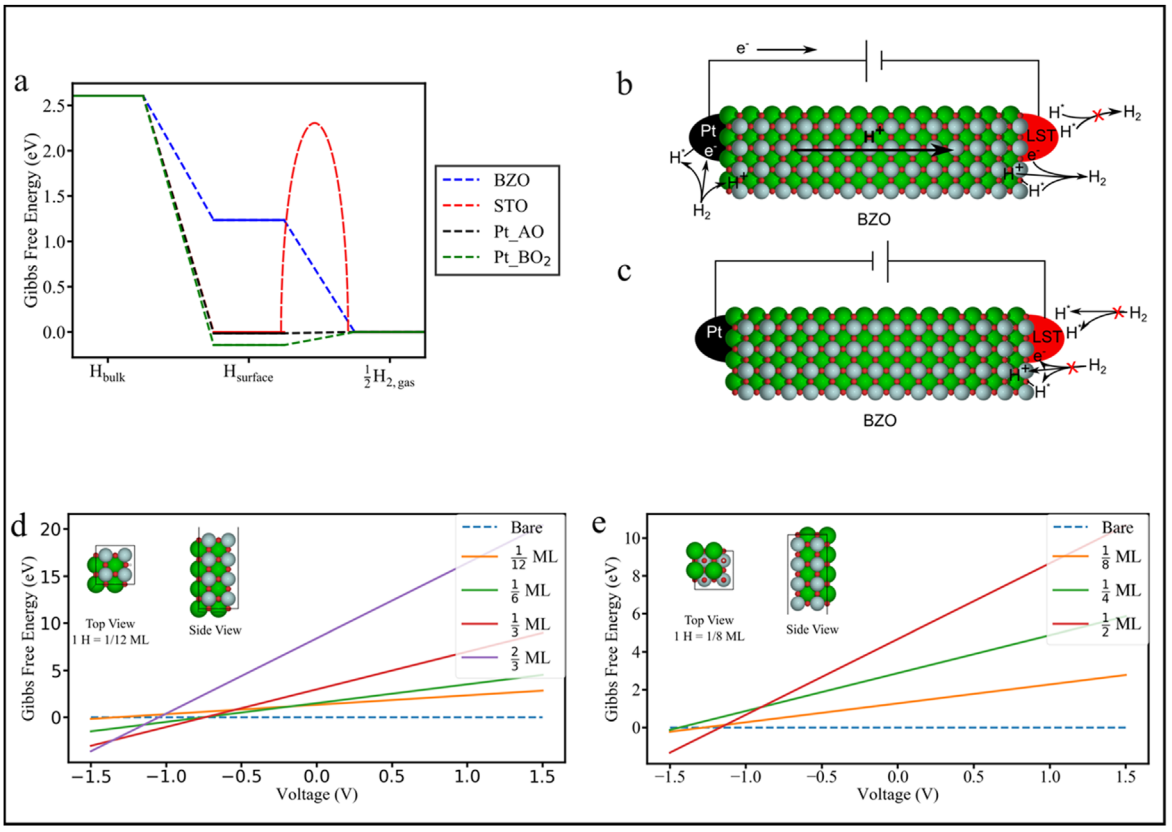

Figure 6. (a) free energy diagram for hydrogen diffusion from the bulk BZO electrolyte to the surface and recombination to form hydrogen gas. (b) and (c) schematic of the Pt/BZO/LST cell operating in both polarization directions. (d) stability diagram for BZO (001) with different hydrogen coverages ZrO_2 terminated and (e) BaO terminated.

The 2 eV activation barrier on STO implies that H_2 dissociation is kinetically inhibited on the LST surface. The only remaining material onto which the hydrogen can adsorb is the electrolyte. The adsorption of H on [001] BZO is thermodynamically uphill by 1.2 eV (see Fig. 6a). We calculated stability diagrams for hydrogen on both [001] BZO surface terminations in order to determine the equilibrium coverage at various applied potentials. H atoms were adsorbed on the surface at different coverages and Eq. 2 was used to calculate the Gibbs free energy relative to the energy of the clean surface at varying potentials (U).

$$\Delta G(U) = \Delta G(0) - neU \quad [2]$$

The results show that hydrogen adsorption on either [001] BZO surface termination is not favorable until reducing potentials of at least −0.7 V (vs SHE) (see Figs. 6d and 6e) confirming that a dissociation catalyst is needed to facilitate hydrogen adsorption from the gas phase. Thus, hydrogen gas cannot dissociate on the LST-BZCYYb electrode and no current is generated for the cell running in this direction.

Discussion

As discussed in the Introduction, the electrochemical production of ammonia in a PCC could have important advantages. One method to accomplish this involves electrolysis to form H_2, followed by a conventional Haber-Bosch process;[22] however, direct utilization of the hydrogen ions that pass through the electrolyte to form ammonia directly could have important advantages in greatly simplifying the process. For this to be practical, high Faradaic efficiencies are essential. This in turn requires electrochemical promotion of the reaction within the electrode.

The best known example of electrochemical promotion of reactions in solid-state devices is the so called NEMCA (Non-Faradaic Electrochemical Modification of Catalytic Activity) effect, sometimes referred to as Electrochemical Promotion of Catalysis (EPOC).[23–25] Presently, the most accepted explanation for the mechanism behind NEMCA is that ions from the electrolyte are pumped onto the catalyst surface upon application of an external potential[26] and that these in turn dramatically enhance the catalytic properties of the electrode. For example, the oxidation of C_2H_4 over Pt electrodes was shown to exhibit electrochemical rate enhancements as large as 3×10^5.[27] Under normal reaction conditions, the Pt surface would become covered with carbonaceous residues at the temperatures and partial pressures used in the study which showed these enhancements. These residues would block sites for O_2 adsorption and limit the reaction. Imbihl and coworkers showed that "Application of a positive potential (to a Pt/ZrO_2 electrode) causes a partial removal of the inhibiting CH_x adlayer by spillover oxygen thus triggering a transition from the poisoned state of the surface to an active state with reduced carbon coverage."[8] Restated, Imbihl demonstrated that oxygen ions introduced to the Pt surface from the electrolyte were much more efficient at removing carbonaceous residues from Pt than was gas-phase O_2.

Applying these principles to the synthesis of NH_3, it should be possible to electrochemically pump hydrogen atoms onto a nitrogen-covered metal to form NH_3. However, to accomplish this, it is essential that H_2 evolution be blocked. What the results in the present work show is that H_2 evolution from BZCYYb electrolyte occurs easily, even in the absence of a catalytic metal. The low barrier for H_2 evolution makes it difficult to use spillover hydrogen effectively.

It is possible that the barrier for H_2 evolution could be higher in other electrolytes. Hydrogen mobility within the electrolyte is required for good conductivity but the calculations shown here make it clear that it is the difference between the energy of the surface protons and those in the bulk that provide the driving force for H_2 production from the electrolyte surface. It is possible that alternative electrolytes or surface modification of BZCYYb could increase this barrier.

The low barrier for H_2 evolution may have implications for materials selection in electrolyzers based on PCC. The conventional electrodes are based on composites of Ni with the electrolyte and Ni is thought to be needed in part for its catalytic properties. If no catalyst is required, other electronic conductors should be equally effective. For example, conductive ceramics, like LST, have advantages due to their intrinsic chemical and thermal stability.

Electrochemical production of chemicals is still a relatively new field and we have much to learn about how to carry out these reactions. The present work provides some insight into the fundamental processes that need to be controlled.

Conclusions

Studies of LST-BZCYYb electrodes demonstrate that a catalytic metal is required for H_2 dissociation but not for H recombination. Both experiments and DFT calculations indicate that the barrier for hydrogen recombination from protons in the bulk electrolyte is low.

Acknowledgments

The author acknowledge support from the National Science Foundation under Grant Nos. (1804145 and 1803758). Any opinions, findings, and conclusions or recommendations expressed in this material are those of the authors and do not necessarily reflect the views of the National Science Foundation. We would also like to thank the following people for their advice and help: Chaehyun Lim, Julian Paige, Tianyu Cao, Hanchen Tian, Jong-Sung Park and Yu-Hao Yeh.

ORCID

Raymond J. Gorte https://orcid.org/0000-0003-0879-715X

References

1. I. A. Amar, R. Lan, C. T. G. Petit, and S. Tao, *J. Solid State Electrochem.*, **15**, 1845 (2011).
2. S. Giddey, S. P. S. Badwal, and A. Kulkarni, *Int. J. Hydrogen Energy*, **38**, 14576 (2013).
3. E. Vasileiou, V. Kyriakou, I. Garagounis, A. Vourros, and M. Stoukides, *Solid State Ionics*, **275**, 110 (2015).
4. R. Schlögl, *Angew. Chemie Int. Ed.*, **42**, 2004 (2003).
5. C. H. Bartholomew and R. J. Ferrauto, *Fundamentals of Industrial Catalytic Processes* (Wiley, United States of America) 380 (2006).
6. J. C. Lin, N. Shamir, Y. B. Zhao, and R. Gomer, *Surf. Sci.*, **231**, 333 (1990).
7. M. Mahnig and L. D. Schmidt, *Zeitschrift für Phys. Chemie*, **80**, 71.
8. A. Toghan, L. M. Rösken, and R. Imbihl, *Phys. Chem. Chem. Phys.*, **12**, 9811 (2010).
9. S. McIntosh, H. He, S.-I. Lee, O. Costa-Nunes, V. V. Krishnan, J. M. Vohs, and R. J. Gorte, *J. Electrochem. Soc.*, **151**, A604 (2004).
10. S. Lee, G. Kim, J. M. Vohs, and R. J. Gorte, *J. Electrochem. Soc.*, **155**, B1179 (2008).
11. S. Park, R. J. Gorte, and J. M. Vohs, *J. Electrochem. Soc.*, **148**, A443 (2001).
12. A. H. Larsen et al., *J. Phys. Condens. Matter*, **29**, 273002 (2017).
13. P. Giannozzi et al., *J. Phys. Condens. Matter*, **21**, 395502 (2009).
14. J. P. Perdew, K. Burke, and M. Ernzerhof, *Phys. Rev. Lett.*, **77**, 3865 (1996).
15. J. D. Pack and H. J. Monkhorst, *Phys. Rev. B*, **16**, 1748 (1977).
16. L. Bengtsson, *Phys. Rev. B*, **59**, 12301 (1999).
17. D. Vanderbilt, *Phys. Rev. B*, **41**, 7892 (1990).
18. H. Jónsson, G. Mills, and K. W. Jacobsen, *Classical and Quantum Dynamics in Condensed Phase Simulations* (World Scientific, Singapore) p. 385 (1998).
19. G. Henkelman, B. P. Uberuaga, and H. Jónsson, *J. Chem. Phys.*, **113**, 9901 (2000).
20. H. Zhu, S. Ricote, C. Duan, R. P. O'Hayre, and R. J. Kee, *J. Electrochem. Soc.*, **165**, F845 (2018).
21. M. Asscher, J. Carrazza, M. M. Khan, K. B. Lewis, and G. A. Somorjai, *J. Catal.*, **98**, 277 (1986).
22. A. Hauch, R. Küngas, P. Blennow, A. B. Hansen, J. B. Hansen, B. V. Mathiesen, and M. B. Mogensen, *Science*, **370**, eaba6118 (2020).
23. C. G. Vayenas, *Solid State Ionics*, **168**, 321 (2004).
24. I. V. Yentekakis, M. Konsolakis, R. M. Lambert, A. Palermo, and M. Tikhov, *Solid State Ionics*, **136–137**, 783 (2000).
25. I. Garagounis, V. Kyriakou, and M. Stoukides, *Solid State Ionics*, **231**, 58 (2013).
26. S. Ladas, S. Kennou, S. Bebelis, and C. G. Vayenas, *J. Phys. Chem.*, **97**, 8845 (1993).
27. S. Bebelis and C. G. Vayenas, *J. Catal.*, **118**, 125 (1989).